NEUROSCIENCE

Optimal focused ultrasound lesion location in essential tremor

Melissa M. J. Chua[1]*, Alfredo Morales Pinzon[2], Clemens Neudorfer[3], Patrick R. Ng[1], Sarah E. Blitz[1], Garance M. Meyer[3], Konstantin Butenko[3], Till A. Dembek[3,4], Alexandre Boutet[5], Andrew Z. Yang[5], Michael Schwartz[6], Jürgen Germann[5], Nir Lipsman[6], Andres Lozano[5,7], Fardad Behzadi[2], Nathan J. McDannold[2], John D. Rolston[1], Charles R. G. Guttmann[2], Michael D. Fox[3], G. Rees Cosgrove[1], Andreas Horn[3,8,9]

Magnetic resonance–guided focused ultrasound (MRgFUS) thalamotomy is an effective treatment for medically refractory essential tremor. We investigate ablation sites and potential tracts associated with optimal tremor control and side effects based on the analysis of 351 cases from three international hospitals. Lesions were segmented on day 1 thin-cut T2 axial images, mapped to standard Montreal Neurological Institute space, and used to derive probabilistic maps and tracts associated with tremor improvement and side effects. Lesioning of a specific subregion within the ventral intermediate nucleus and the cerebellothalamic tract was associated with optimal tremor improvements. Some lesion locations and tracts were associated with differential side effects. Overlaps with the optimal tremor improvement sites accounted for variance in clinical improvements in out-of-sample cases. Efficacy of this location was further confirmed by test-retest cases that underwent two MRgFUS procedures. We identify and validate a target area for optimal tremor control and sites of avoidance associated with side effects.

INTRODUCTION

Essential tremor (ET) is a common movement disorder that affects about 7 to 10 million people in the United States and 0.9% of people globally (*1*, *2*). While medical management is the first-line treatment, there remains a large subset of patients who are refractory to medications or unable to tolerate medication side effects (*3*). Transcranial magnetic resonance–guided focused ultrasound (MRgFUS) thalamotomy of the ventral intermediate nucleus (Vim) allows targeting and incisionless lesioning with real-time monitoring using MR thermometry for medically refractory ET, particularly in patients with contraindications to or with personal preferences against deep brain stimulation (DBS) (*4*). Long-term outcomes at 5 years after MRgFUS thalamotomy have shown persistent substantial benefit in tremor control without delayed occurrence or worsening of posttreatment complications (*5*).

The Vim borders the internal capsule laterally and sensory thalamic nuclei posteriorly (*6*). Thus, targeting the "optimal" location, including lesion size and shape, is important for tremor control while avoiding adverse effects. Novel imaging sequences such as white matter nulled magnetization prepared rapid acquisition gradient echo, white matter attenuated inversion recovery, fast gray matter acquisition T1 inversion recovery, and susceptibility-weighted imaging have been used in an attempt to directly visualize thalamic nuclei and, particularly, the Vim (*7*–*9*). However, to date, there is no optimal or standardized protocol for targeting.

[1]Department of Neurosurgery, Brigham and Women's Hospital, Harvard Medical School, Boston, MA, USA. [2]Department of Radiology, Brigham and Women's Hospital, Harvard Medical School, Boston, MA, USA. [3]Department of Neurology, Brigham and Women's Hospital, Harvard Medical School, Boston, MA, USA. [4]Department of Neurology, Faculty of Medicine, University of Cologne, Cologne, Germany. [5]University Health Network, Toronto, ON, Canada. [6]Division of Neurosurgery, Sunnybrook Health Sciences Centre, University of Toronto, Toronto, ON, Canada. [7]Krembil Research Institute, Toronto, ON, Canada. [8]Department of Neurosurgery, Massachusetts General Hospital, Harvard Medical School, Boston, MA, USA. [9]Institute for Network Stimulation, Department of Stereotactic and Functional Neurosurgery, University Hospital Cologne, Germany.
*Corresponding author. Email: mchua@bwh.harvard.edu

Diffusion magnetic resonance imaging (dMRI)–based tractography can help identify specific white matter tracts that may be important for understanding outcomes, and possibly even for targeting. In recent years, there has been growing interest in the cerebellothalamic tract (CTT) as the target for optimal tremor control (*6*, *10*–*12*). However, the results have not been validated in large cohorts to propose a shift toward tractography-based targeting (*13*–*15*). Furthermore, diffusion sequences are typically based on echo-planar imaging, which is prone to stark distortion artifacts and poor resolution (1.5 to 2.0 mm isotropic) which render individualized dMRI scans problematic for precise stereotactic targeting (*16*, *17*).

Normative high-quality tractograms in association with clinical outcomes analyzed through statistical applications may lend insight into tracts that could play a role in MRgFUS targeting, but which are currently difficult if impossible to reconstruct using patient-level dMRI data (*18*–*20*).

Consequently, most centers still rely upon atlas-based coordinates with adjustments for individual variations based on real-time intraoperative MRI. Small adjustments are made throughout the procedure based on individual patients' clinical responses to low-energy test sonications before ablative sonications (*21*).

To date, a small number of studies have investigated the optimal location for tremor control with small cohorts by using probabilistic mapping of ablative effects, a process termed "sweetspot mapping" (*22*, *23*). In general, they substantiate the notion that the Vim proper, or its ventral border (into which cerebellar projections fibers enter), would serve as the optimal target for tremor control. However, little quantitative evidence regarding sites associated with the occurrence of side effects is known, and studies on large cohorts are lacking.

Here, we investigate sites associated with optimal tremor control and side effects following ablation based on a large cohort of patients with medically refractory ET who underwent unilateral MRgFUS thalamotomy. This led to a set of "sweet" and "sour" spots for MRgFUS targeting which we investigate further based on patients that underwent re-treatment due to tremor recurrence. Further, we apply the

fiber filtering method to investigate which tracts associate with optimal outcomes and occurrence of side effects (*24*). We test whether overlaps between lesions and the identified optimal sonication location accounts for clinical improvements in independent hold-out test cohorts from the same and other centers.

RESULTS

Patient characteristics and tremor outcomes

Patient demographics and tremor scores are reported in Table 1 and consisted of a discovery cohort ($n = 200$) that was prospectively collected at Brigham and Women's Hospital (BWH) in Boston, MA and was used to calculate sweet- and sourspots (tremor improvements and side effects). The main result (tremor sweetspot) was further validated using two additional independent test cohorts; a first additional cohort from BWH ($n = 102$), as well as a cohort of cases that underwent MRgFUS thalamotomy in Toronto ($n = 49$). BWH Discovery Cohort ($n = 200$): Mean age was 75.3 ± 7.3 years (range, 53 to 94) and 68% were male. The average disease duration was 27.6 ± 18.2 years (range, 2 to 70). The majority of patients were right-handed (83.5%), and most underwent left-sided thalamotomy (81.5%). Baseline FTM tremor scores ($n = 200$) were 7.1 ± 2.5 (range, 3 to 16), with overall mild head and voice tremor, and more marked hemi-postural (2.6 ± 0.82) and hemi-intention (3.3 ± 0.68) tremor. Tremor was reduced by 94.9 ± 9.0% at postoperative day 1 ($n = 199$) and 91.6 ± 18.3% at 3 months ($n = 162$). One year post-procedure ($n = 152$), the average FTM tremor score reduction remained significant and was 86.0 ± 26.6% ($P < 0.001$). Similarly, the average percent FTM intention tremor reduction was 82.8 ± 29.7% ($P < 0.001$). Intraoperative sonication parameters are reported in table S1. BWH Validation Cohort ($n = 102$): Mean age was 74.0 ± 6.1 years (range, 59 to 92) and 72.5% were male. Most patients were right-handed (80.4%) and most underwent left-sided thalamotomy (74.5%). Baseline FTM tremor scores were 6.6 ± 2.0 (range, 3 to 14). Tremor was reduced by 95.4 ± 13.7% at 3 months ($n = 86$) and 91.7 ± 19.2% at 1 year ($n = 53$). Toronto Validation Cohort ($n = 49$): Lesion segmentations of this cohort, which received sonications at either Toronto Western Hospital (TWH; $n = 35$) or Sunnybrook Health Sciences Centre (SHSC; $n = 14$) have been previously published by Boutet *et al.* (*23*). However, while the prior publication reported on 3-month outcomes, in the meantime, 12-month outcomes became available for these cases, which were additionally included here. Mean age was 69.4 ± 8.6 years (range, 42 to 85) and 71.4% were male. Most underwent left-sided thalamotomy (85.7%).

Tremor improvements and lesion location and intersection with the CTT

We identified a subregion within the Vim, which was associated with optimal 1-year FTM score improvements (Fig. 1) and was significant after Bonferroni correction ($P < 0.05$). To probe how much

Table 1. Patient characteristics and tremor outcomes. FTM, Fahn-Tolosa-Marin.

	BWH discovery ($n = 200$)	BWH validation ($n = 102$)	Toronto validation ($n = 49$)
Age, years	75.27 ± 7.32 (53–94)	73.98 ± 6.18 (59–92)	69.41 ± 8.60 (42–85)
Male (%)	136 (68.0%)	74 (72.5%)	35 (71.4%)
Disease duration, years	27.62 ± 18.22 (2–70)	24.90 ± 18.40 (3–68)	NA
Dominant hand (%)			
Left	28 (14%)	19 (18.6%)	NA
Right	167 (83.5%)	82 (80.4%)	NA
Ambidextrous	5 (2.5%)	1 (1%)	NA
Treatment laterality (%)			
Left	163 (81.5%)	76 (74.5%)	42 (85.7%)
Right	37 (18.5%)	26 (25.5%)	7 (14.3%)
FTM score (postural)			
Baseline	2.64 ± 0.82 (0–4)	2.69 ± 0.84 (1–4)	2.53 ± 0.97 (0–4)
1 day	0.04 ± 0.18 (0–1) ($n = 199$)	0.04 ± 0.19 (0–1)	NA
3 months	0.11 ± 0.50 (0–4) ($n = 164$)	0.03 ± 0.18 (0–1) ($n = 86$)	0.73 ± 0.90 (0–4)
1 year	0.22 ± 0.70 (0–4) ($n = 152$)	0.17 ± 0.47 (0–2) ($n = 53$)	0.86 ± 0.86 (0–3)
FTM score (intention)			
Baseline	3.25 ± 0.68 (1–4)	3.06 ± 0.76 (1–4)	2.57 ± 0.83 (0–4)
1 day	0.23 ± 0.47 (0–2) ($n = 199$)	0.03 ± 0.17 (0–1)	NA
3 months	0.34 ± 0.79 (0–4) ($n = 164$)	0.17 ± 0.46 (0–2) ($n = 86$)	1.22 ± 0.90 (0–4)
1 year	0.58 ± 1.03 (0–4) ($n = 152$)	0.32 ± 0.64 (0–3) ($n = 53$)	1.29 ± 1.05 (0–4)
FTM score (total)			
Baseline	7.06 ± 2.45 (3–16)	6.60 ± 1.95 (3–14)	7.88 ± 2.93 (3–17)
1 day	0.42 ± 0.84 (0–5) ($n = 199$)	0.16 ± 0.54 (0–4)	NA
3 months	0.70 ± 1.73 (0–12) ($n = 164$)	0.29 ± 0.76 (0–4) ($n = 86$)	3.09 ± 2.51 (0–10)
1 year	0.99 ± 1.94 (0–10) ($n = 152$)	0.55 ± 1.25 (0–7) ($n = 53$)	3.79 ± 2.53 (0–9)

variance in tremor improvements the sweetspot could potentially explain in this large sample of patients, we first carried out a circular analysis that overlaid each lesion with the sweetspot volume. These overlaps explained 15% of the variance in tremor outcomes ($R^2 = 0.15$). We refrain from providing a P value because the analysis was circular. The analysis remained robust when subjected to 10-fold cross-validation ($R = 0.23$, $P = 0.005$). Repeating the analysis in a split-half design continued to demonstrate the robustness of the model ($R = 0.22$, $P = 0.005$). Lesion volumes (sizes) were also significantly correlated with 1-year FTM score improvement ($R = 0.16$, $P = 0.048$). However, when jointly analyzed in a linear model, (10-fold CV) overlaps with the sweetspot but not lesion volume remained significant ($P < 0.001$ versus $P = 0.27$).

The identified sweetspot intersected with the CTT as defined by either of the two tract atlases we used (fig. S1). To test this further, we analyzed which tracts would associate with tremor improvements in a data-driven fashion using fiber filtering. From the entire set of possible streamlines in the two tract atlases, streamlines that formed part of the CTT contributed the majority of streamlines positively associated with tremor improvements and remained significant after Bonferroni correction ($P < 0.05$). The peak t value was 4.34, discriminating tremor improvements from lesions that intersected versus those that did not intersect the streamline. Data-driven tracts that associated with maximal tremor improvements are shown in Fig. 2 for the DBS Tractography Atlas v2 and reproduced for the Basal Ganglia Pathway Atlas (peak t value 4.68) in fig. S2. Overlaps between lesions and identified tracts positively correlated with tremor improvements ($R = 0.29$, DBS Tractography Atlas; $R = 0.26$, Basal Ganglia Pathway Atlas). However, this analysis is circular (thus, we refrain from reporting P values) and was hence repeated in a 10-fold cross-validation design that also showed significant results ($R = 0.24$, $P = 0.004$, DBS Tractography Atlas; $R = 0.20$, $P = 0.015$, Basal Ganglia Pathway Atlas). Results also remained significant when subjected to a split-half design ($R = 0.23$, $P = 0.004$, DBS Tractography Atlas; $R = 0.19$, $P = 0.018$, Basal Ganglia Pathway Atlas).

Side effects and lesion location

The frequency of side effects at each follow-up time point post-MRgFUS on day 1, 3 months, and 1 year is reported in Table 2 and summarized graphically in fig. S3. Side effects at postoperative day 1 were defined as acute and those at 3 months and beyond were defined as persistent. At postoperative day 1, the most common side effect was gait imbalance (63.3%) followed by sensory deficits (mostly in the lip and/or tongue area) (24.6%), dysarthria (16.6%), and weakness (10.6%). At 3 months and 1 year, gait imbalance remained the most common side effect (26.7 and 17.1%, respectively). All side effects were mild (Clavien-Dindo grade I), largely subjective (particularly for gait imbalance), and gradually resolved over time (*25*). On the basis of the currently available 4-year outcomes from our database, of 46 patients, none reported weakness (0%), 2 had

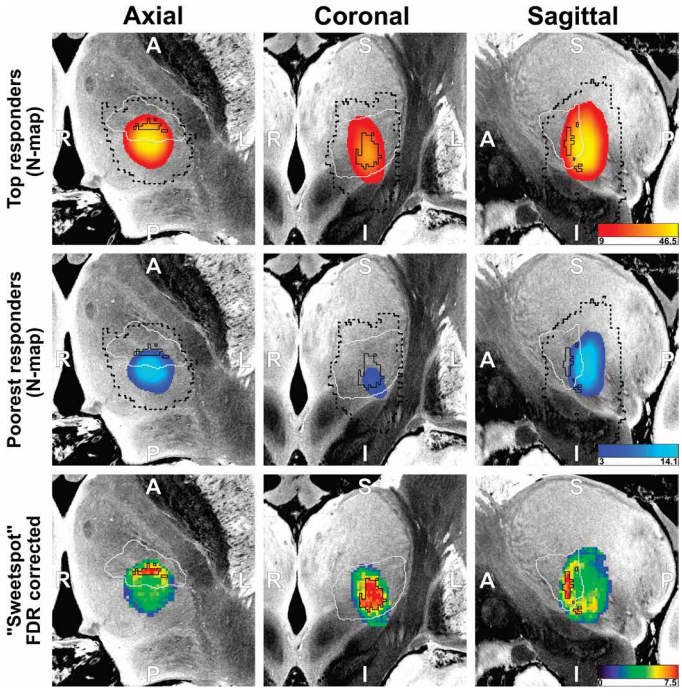

Fig. 1. Sweetspot results. Area associated with optimal tremor control at 1-year post-MRgFUS thalamotomy. N-map of the top responders at 1 year ($n = 62$) defined as 100% improvement in FTM tremor score (subitems of part A, see Materials and Methods) and of the poorest responders at 1 year ($n = 11$) defined as <50% improvement in FTM tremor score (second row). The entire area covered by lesions ($n = 200$) is outlined by the dotted black lines. The sweetspot area of optimal tremor control (bottom row, FDR-corrected $P < 0.05$) was determined based on the 1-year post-MRgFUS thalamotomy FTM improvement, where the average improvement in our cohort was 86.0%. The Bonferroni-corrected area ($P < 0.05$) is outlined by the black solid lines. This same area is superimposed on the N-maps of the top and poorest responders to demonstrate their spatial relationships with the peak region of the sweetspot. The Vim (based on the DISTAL atlas) is defined by the white outline (*61*). Color bars in the first two rows represent number of patients, while color bar in the last row represents the z (signed rank) statistic.

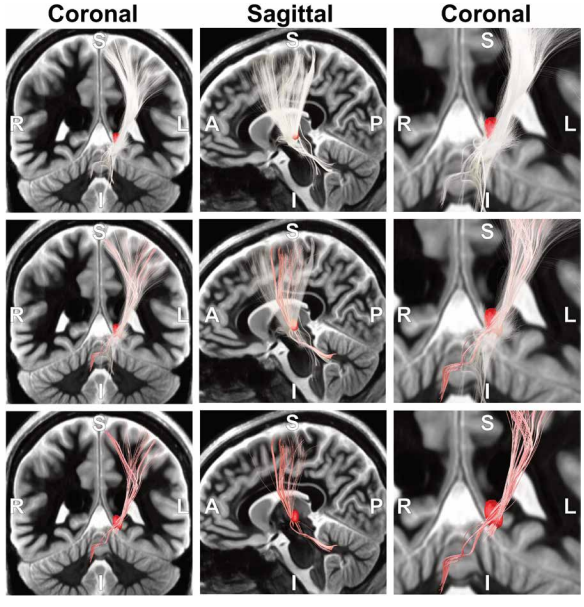

Fig. 2. Fiber filtering results. All tracts within the DBS Tractography Atlas, v2 are shown in white (top and middle rows). Tracts associated with optimal tremor control (FDR corrected) at 1-year post-MRgFUS thalamotomy are shown in red (t value = 3.86 to 4.34), of which majority (70%) correspond to the cerebellothalamic tract (middle and bottom rows). A thresholded version of the N-map showing the site where lesions were mostly created is shown as the red volume.

Table 2. Adverse events.

	1 day (n = 199)	3 months (n = 164)	1 year (n = 152)
Weakness	21 (10.55%)	10 (6.21%)	6 (3.95%)
Face	8 (4.02%)	2 (1.24%)	0
Upper extremity	4 (2.01%)	2 (1.24%)	0
Lower extremity	11 (5.53%)	7 (4.35%)	6 (3.95%)
Sensory deficits (paresthesias/ numbness)	49 (24.62%)	43 (26.71%)	22 (14.47%)
Orofacial (lips and/or tongue)	44 (22.11%)	41 (25.47%)	22 (14.47%)
Fingers	18 (9.05%)	11 (6.83%)	6 (3.95%)
Gait imbalance	126 (63.32%)	43 (26.71%)	26 (17.11%)
Dysarthria	33 (16.58%)	6 (3.73%)	7 (4.61%)
Dysgeusia	NA	19 (11.80%)	15 (9.87%)
Any side effect	151 (75.88%)	86 (52.44%)	57 (37.50%)

dysarthria (4.3%), 4 had sensory changes (8.7%), and 5 reported mild imbalance (10.9%).

We identified specific areas (sourspots) and tracts associated with the occurrence of each side effect at 1-day post-MRgFUS (Figs. 3 and 4; dysgeusia is shown at 3 months because the outcome was not collected at day 1 in all patients). We found that sensory side effects and dysgeusia were associated with lesions extending posteriorly and medially into the ventral posterolateral (VPL) and ventral posteromedial (VPM) nuclei. Weakness was associated with lesions extending laterally into the internal capsule. Dysarthria was associated with lesions extending superomedially, and gait imbalance associated with lesions extending ventrolaterally toward the inferior region of the Vim. All sourspots and tracts were significant after Bonferroni correction ($P < 0.05$) except dysarthria and dysgeusia, which were only significant at the uncorrected level ($P < 0.05$). There were substantially fewer patients with persistent side effects (3 months and beyond). Temporal stability of the sourspot analysis was hence only tested for sensory side effects, which were frequent enough to calculate statistics at the 3-month and 1-year time points. Maps showed stability over time, pointing to the posteriorly adjacent sensory thalamic nuclei (fig. S4).

Quantitative analysis of tracts revealed 100% correspondence to medial lemniscus for sensory deficits, 52% to corticospinal tract (CST) for weakness, 44% to CTT and 16% corresponding to CST for imbalance, and 55% corresponding to trigeminothalamic tract and medial lemniscus for dysgeusia. There was no clear single tract that could be identified for dysarthria. We used a 10-fold cross-validation approach to validate our observations of the side effects that remained significant following post hoc correction (i.e., weakness, sensory deficits, and gait imbalance; all $P < 0.05$). Repeating the analysis in a split-half design demonstrated the robustness of our model (all $P < 0.05$).

The average lesion volume in our cohort was 462.90 ± 190.15 mm^3. Mean lesion volumes of the patients with a side effect were significantly larger than those without at every time point (1 day postoperative, 494.99 ± 186.09 versus 364.01 ± 164.82; 3 months, 540.63 ± 168.76 versus 389.26 ± 154.18; 1 year, 520.54 ± 182.66 versus 407.45 ± 157.28 mm^3; all $P < 0.001$). When analyzing specific side effects across all time points, patients with each respective side effect had significantly larger lesions than those without the same side effect 1 day after surgery (all $P < 0.05$). When restricting the analysis to the 3-month postoperative time point, only patients with weakness, imbalance, or sensory deficits had significantly larger lesions than patients who did not ($P < 0.05$). When restricting the analysis to the 1-year postoperative time point, only patients with imbalance had significantly larger lesions than those without ($P < 0.05$).

Out-of-sample validation

To test whether the identified sweetspot would generalize to additional patients (including patients treated at different centers), we calculated the average weighted lesion overlaps of the BWH and Toronto validation cohorts with the sweetspot [thresholded at false discovery rate (FDR) significance]. This coefficient was correlated with empirical outcomes with the idea that high overlap scores should lead to high tremor improvements. In the BWH validation cohort (n = 102), weighted average overlaps between their lesions in respective patients significantly correlated with empirical percentage tremor improvements at both time points (3 months: $R = 0.27$, $P = 0.012$; 1 year: $R = 0.42$, $P = 7.9 \times 10^{-4}$). In the Toronto validation cohort (n = 49), weighted average overlaps again significantly correlated with clinical improvements (3 months: $R = 0.29$, $P = 0.041$; 1 year: $R = 0.32$, $P = 0.033$). Correlations between the weighted sweetspot lesion overlaps and tremor improvements across the entire test cohort (BWH and Toronto combined; $N = 151$) also led to significant findings for both percentage ($R = 0.63$, $P = 2.0 \times 10^{-4}$) and absolute tremor improvements ($R = 0.48$, $P = 10^{-2}$; Fig. 5).

Patient-specific examples

Six patients underwent re-treatment at our institution after an unsuccessful first MRgFUS thalamotomy due to failure to sustain tremor improvement. We visualized the location of our sweetspot in relation to the lesions on their postoperative day 1 MRI (Fig. 6, A and B). To test whether outcome changes across the two treatments could be explained by overlaps of respective lesions with the sweetspot, we first recalculated the sweetspot without these six patients to avoid circularity. Overlaps of zone 1 with the sweetspot were, on average, larger in the group that had sustained tremor

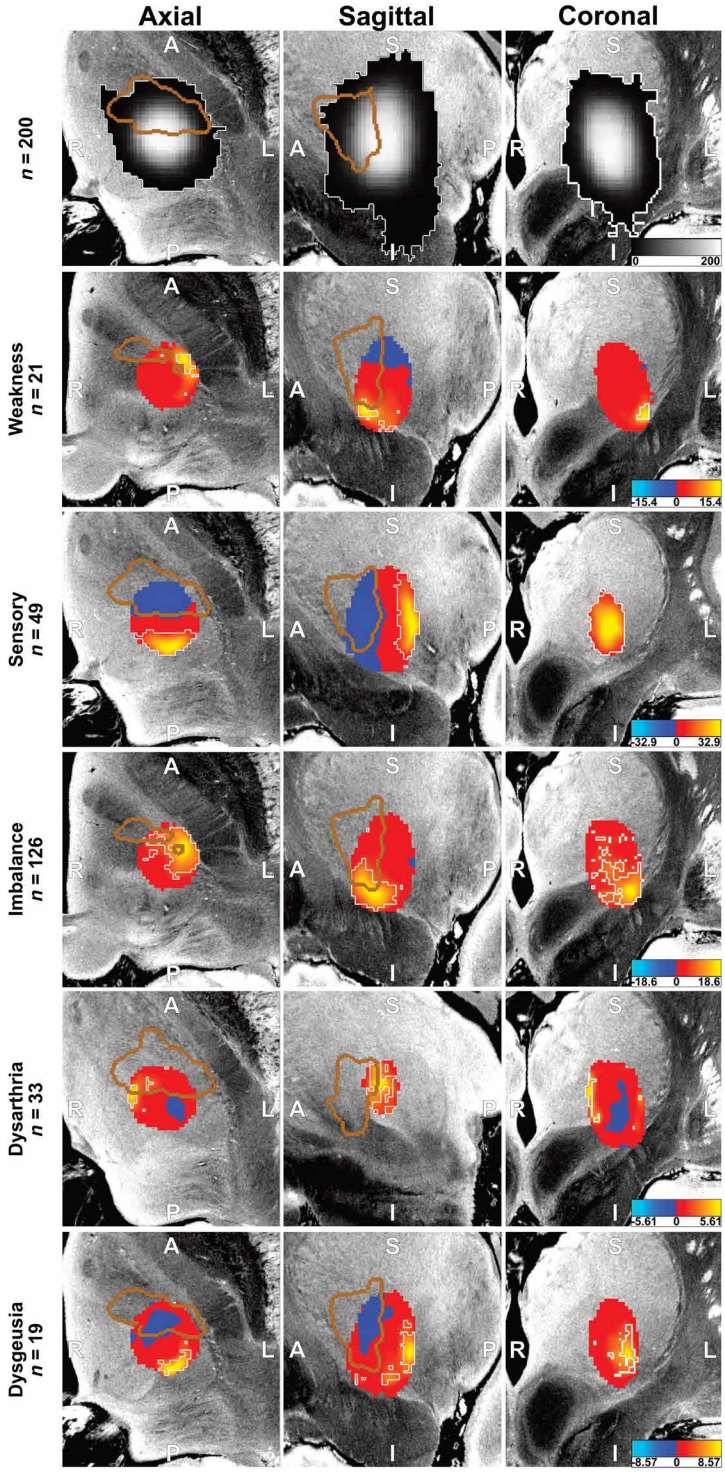

Fig. 3. Sourspots associated with side effects. Areas associated with side effects at 1-day post-MRgFUS thalamotomy (except dysgeusia, which is shown at 3 months because the outcome was not collected at 1-day postprocedure). The N-map of all lesions is shown in the top row (n = 200). The sourspot of each side effect is shown in hot colors, and voxels negatively associated with the occurrence of the side effect are in cold colors. The FDR-corrected area ($P < 0.05$) is outlined in white for weakness, sensory deficits, and imbalance. The significant area at the uncorrected level ($P < 0.05$) is outlined in white for dysarthria and dysgeusia as they were not significant with FDR correction. The Vim (based on the DISTAL atlas) is defined by the brown outline in the axial and sagittal planes. The color bar in the first row represents number of patients, while color bars in the other rows represent the statistic value for the proportion test.

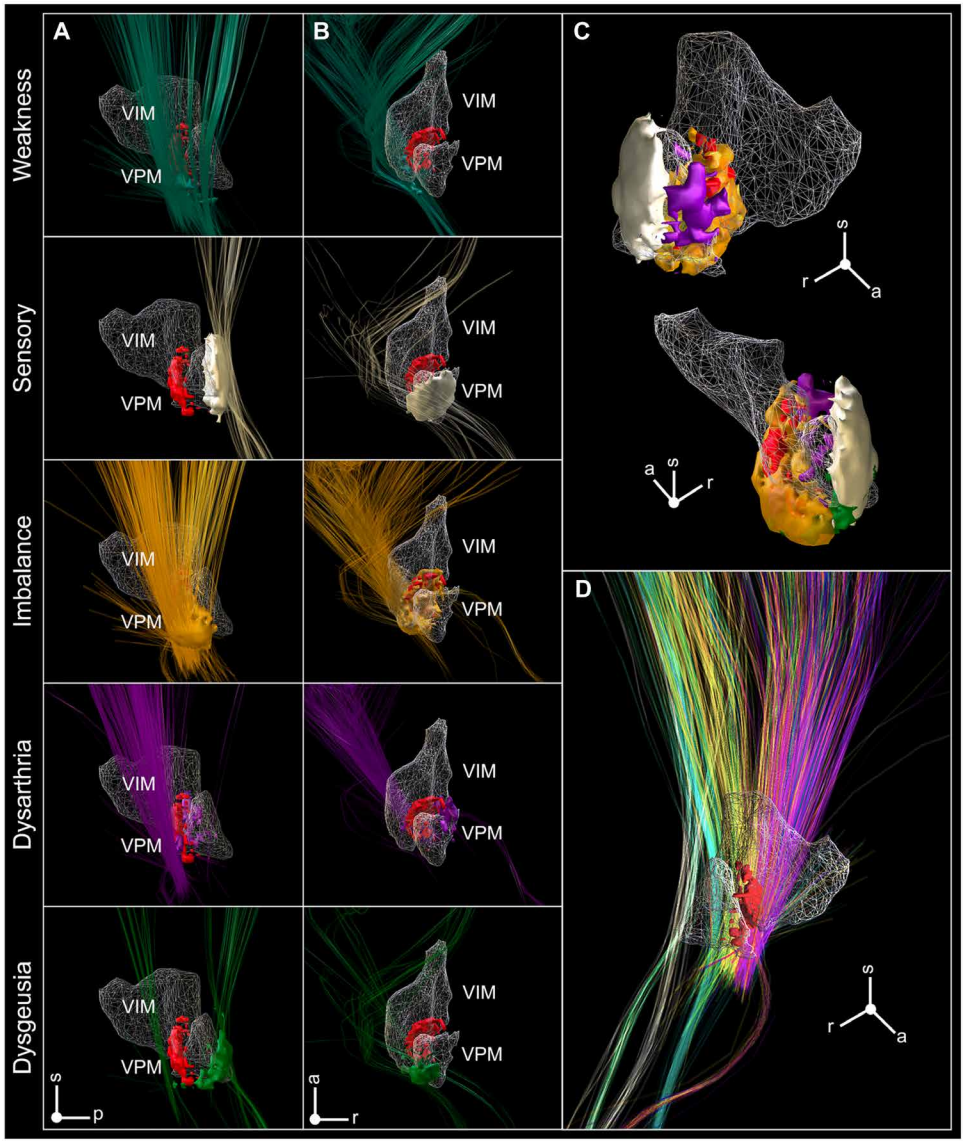

Fig. 4. Tracts and sourspots associated with each type of side effect. Tracts shown at an FDR-corrected significant level ($P < 0.05$) for weakness (dark green), sensory deficits (beige), and imbalance (yellow); shown at a significant level ($P < 0.05$) uncorrected for multiple comparisons for dysarthria (purple) and dysgeusia (green) in relation to the sweetspot (red) and each side effect's respective sourspot. The Vim (based on the DISTAL atlas) is shown as a white wireframe. a = anterior; p = posterior; r = right; s = superior. (**A**) and (**B**) show views from lateral (sagittal view) and top (axial view), respectively. (**C**) shows sourspots and (**D**) fiber tracts of all types of side effects together (again including the optimal tremor response sweetspot in red).

control after re-treatment, compared to the group that did not (14.3% versus 6.4%) (Fig. 6C). Overlap of zone 1 with the sweetspot was significantly higher in the second treatment compared to the first treatment in the group that had sustained tremor control after re-treatment ($P = 0.028$); on the other hand, there was no significant change in overlap of zone 1 by the lesion from treatment 1 versus treatment 2 in the group that did not have improved tremor control after re-treatment ($P = 0.82$). Further, we screened the entire cohort ($n = 152$) of patients that had 0% FTM tremor improvements at 1 year, which was rare (8 patients, i.e., 5.3%) and hence made this subset of patients a specific set of cases to learn from. In Fig. 6D, we show lesions on postoperative day 1 of these patients together with the sweetspot. Lesions in these patients had little to no overlap with the sweetspot. Figure S5 shows the tremor sweetspot warped into native space of three patient examples to compare its location to individual brain anatomy.

Comparison to other published MRgFUS thalamotomy and DBS sweetspots

We compared our sweetspot to other published optimal MRgFUS thalamotomy targets, the traditional Guiot target, as well as published Vim-DBS sweetspots to determine their spatial relationships (Fig. 7 and Table 3) (*22*, *23*, *26*). The MRgFUS study by Federau *et al.* (*22*) included seven patients with an average tremor improvement score [based on the Clinical Rating Scale for Tremor (CRST)] on the treated side of 55 ± 24% at 1 year postprocedure. They correlated the

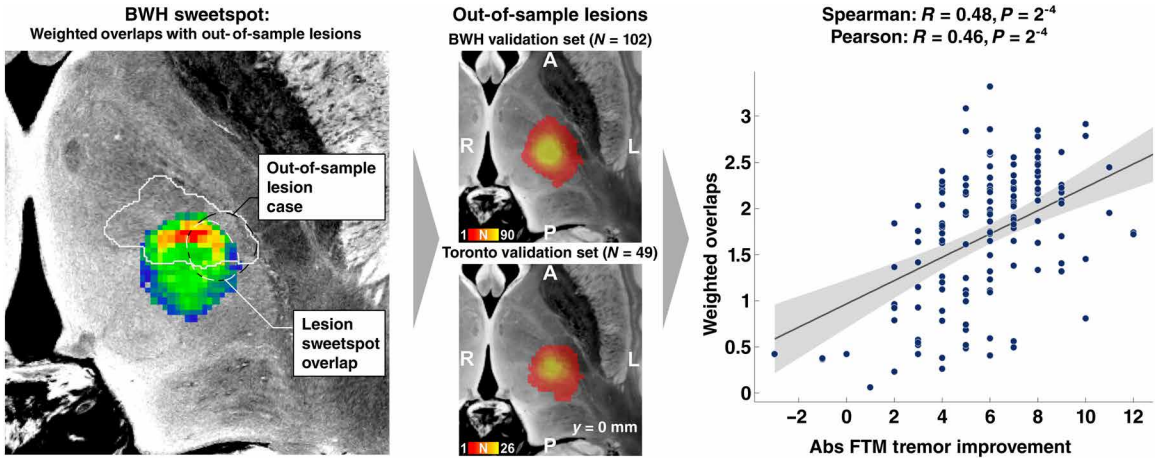

Fig. 5. Validation of sweetspot by out-of-sample cases. Weighted average overlaps between the out-of-sample validation cases and the identified sweetspot were calculated (left) based on $N = 102$ independent cases from BWH and $N = 49$ cases that underwent MRgFUS thalamotomy at two hospitals in Toronto (middle). There were significant correlations between the weighted sweetspot lesion overlaps and tremor improvements at 3-month and 1-year time points in the independent BWH cases ($R = 0.27$, $P = 0.012$; $R = 0.42$, $P = 7.9 \times 10^{-4}$), as well as for the Toronto cohort (3 months: $R = 0.29$, $P = 0.041$, 1 year: $R = 0.32$, $P = 0.033$). Correlations between the weighted sweetspot lesion overlaps and tremor improvements across the entire test cohort (BWH and Toronto combined; $n = 151$) also led to significant findings for both percentage ($R = 0.63$, $P = 2.0 \times 10^{-4}$) and absolute tremor improvements ($R = 0.48$, $P = 10^{-2}$; right).

lesion locations (based on 1-year postprocedural T2-weighted MRI) and clinical outcomes and determined an anterior commissure–posterior commissure (AC-PC) coordinate (*X*: 14.3 mm, *Y*: 8.3 mm, *Z*: 0) associated with maximal clinical benefit. This coordinate was transformed to Montreal Neurological Institute (MNI) space for direct comparison (MNI *X*: −13.78 ± 1.07 mm, *Y*: −16.26 ± 0.82 mm, *Z*: −2.89 ± 0.69 mm). Boutet *et al.* (*23*) included 66 patients in their study with an average CRST improvement of 42 ± 22% at 3 months postprocedure to determine the area associated with best clinical outcomes after 3 months. We refrain from discussing the numerous DBS studies in depth here but refer to Table 3 and prior work that discussed these target sites (*27*, *28*).

DISCUSSION

Our study confirms that MRgFUS thalamotomy is an effective treatment for medically refractory ET with an average overall FTM improvement of 86.0% at 1-year postprocedure. Thirty-seven percent of patients reported adverse effects, but these were mild and temporary in the majority of cases. Larger lesion sizes were associated with stronger tremor improvement but also with the occurrence of side effects, suggesting a cost-benefit trade-off. We identified a target area within the Vim that could significantly differentiate cases with optimal versus suboptimal outcomes of tremor control at 1 year. This analysis alongside individual patient cases that underwent retreatment for tremor recurrence suggest that this sweetspot may have clinical value in guiding MRgFUS thalamotomies going forward. On a tract level, lesioning the CTT was associated with maximal 1-year tremor control. It is important to note that both the Bonferroni-corrected sweetspot and tract targets identified here maximally differentiate top from poor responders and hence may be part of the criteria for successful treatments in our cohort (i.e., the critical volume that needs to be lesioned). However, for statistical reasons, it remains unclear whether the lesion needs to extend to other surrounding areas (i.e., the voxels where all patients had a lesion) that are additionally required to lesion for optimal tremor control. Thus, the FDR-corrected sweetspot can be seen as an optimal lesion, and the Bonferroni-corrected area can be seen as a critical volume to be included in the lesion but not the sole volume to be lesioned. We also additionally validated our sweetspot with out-of-sample data from both within and outside our institution. While our study was not designed to compare outcomes across sites, there were differences in average clinical improvements but also lesion sites and lesion sizes between the BWH and Toronto centers (average lesion size in BWH cohort was 458.4 mm^3 compared to 239.5 mm^3 in the Toronto cohort on the 24-hour postoperative T2-weighted MRI images). Last, we identified areas associated with higher risks of side effects (sourspots). Together, sweet- and sourspots may help in MRgFUS targeting going forward, with the aim of maximizing tremor benefit while minimizing side effects.

When directly compared to sweetspots published in the literature, the area associated with maximal optimal tremor benefit resides in close proximity but slightly anterior to the one reported by Boutet *et al.* (*23*) and superior to the one published by Federau *et al.* (*22*). However, the centroid of the FDR-corrected sweetspot is similar in location to the Boutet *et al.* sweetspot (Table 3). This could mean that the anteriorly situated sweetspot defined by the Bonferroni significance line may be a necessary target, but not sufficient target, i.e., while the anterior portion should be covered by the lesion, it may not be sufficient or advisable to place the center of the lesion onto this spot. The variability in target areas could be due to the differences in surgical targeting (i.e., different centers of target) or methodology in analysis; Boutet *et al.* (*23*) used 3-month postprocedural outcomes for their analysis, while Federau *et al.* (*22*) used imaging at 1 year postprocedure for their lesion analysis. Of note, a recent study showed that lesions may not be visible on imaging at 1-year post-MRgFUS (*29*). Both based their analysis on significantly fewer patients (Federau $n = 7$; Boutet $n = 66$). We demonstrate that our target area was consistently missed in the $n = 8$ patients in our sample who had tremor recurrence at 1 year. Furthermore, our series included six patients that underwent re-treatment after an unsuccessful first treatment. In these, the subset of cases that benefited

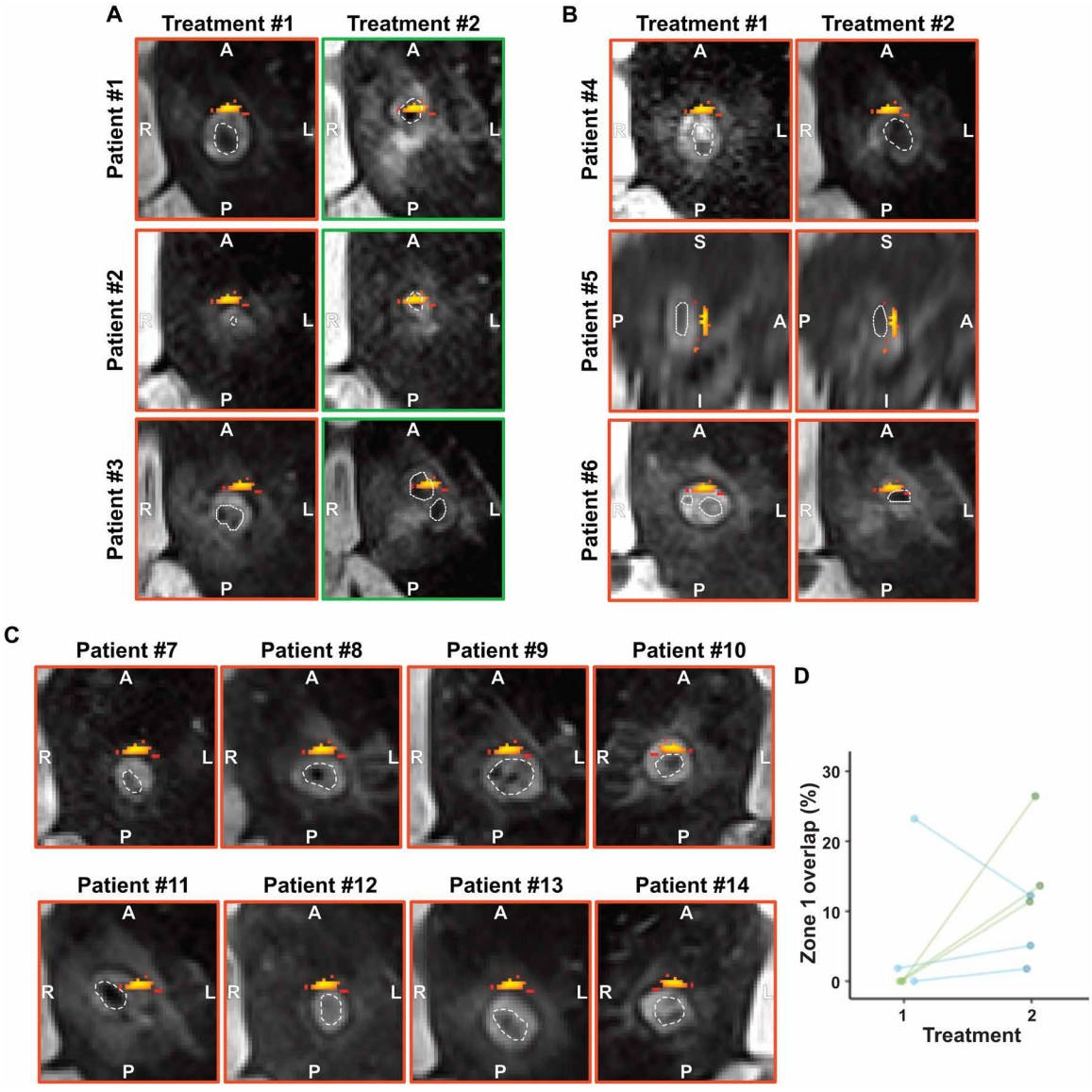

Fig. 6. Individual cases. Postoperative day 1 T2-weighted MRIs with Wintermark zone 1 outlined in white and the Bonferroni-corrected sweetspot overlaid in red/yellow. Patients with (**A**) successful retreatment (green outline) and (**B**) unsuccessful retreatment (red outline). (**C**) Patients with 0% FTM tremor improvement at 1 year. (**D**) Comparison between the percent of overlaps between our sweetspot (recalculated without these six patients) and Wintermark zone 1 of lesions from treatments 1 and 2 color coded for patients who had sustained tremor control after second treatment (green) versus patients who did not (blue).

from re-treatment had significantly higher overlaps of the second lesion with our target area, while those who had unsuccessful re-treatment did not.

Our group has previously reported on the relationship between side effects and lesion direction in a smaller cohort using lesion volumes calculated by measuring each axis (*30*). Here, we build upon this analysis with a larger cohort of patients and a methodology that builds on research in the DBS literature (*31*). We observe that acute and persistent sensory deficits were significantly associated with posterior lesion extension into the VPL and VPM nuclei, which is in line with a priori anatomical knowledge of this area (*32*). Sensory side effects were also associated with lesions of the medial lemniscus, which is similarly in line with our understanding. Our results do not confirm a topographic relationship to the sensory homunculus of the VPL nucleus; however, this could be due to the fact that, in our study, many patients had sensory deficits in more than one body location, lowering the power for separate analysis of thalamic area for each sensory deficit location (*33*). Expectedly, weakness was significantly associated with lesions that extended laterally into the internal capsule and tract analysis associated the effect with lesions of the CST. Imbalance was significantly associated with ventrolateral lesions, with lesioning of the CTT followed by CST associated most strongly. This could represent gait imbalance arising due to motor leg weakness from lesion extension into the CST, or cerebellar disturbance from extension into the CTT. In addition, the location of the imbalance sourspot could also reflect the lateral Vim area, which represents the homuncular leg area of Vim (fig. S6). Slight posterior extension of the imbalance

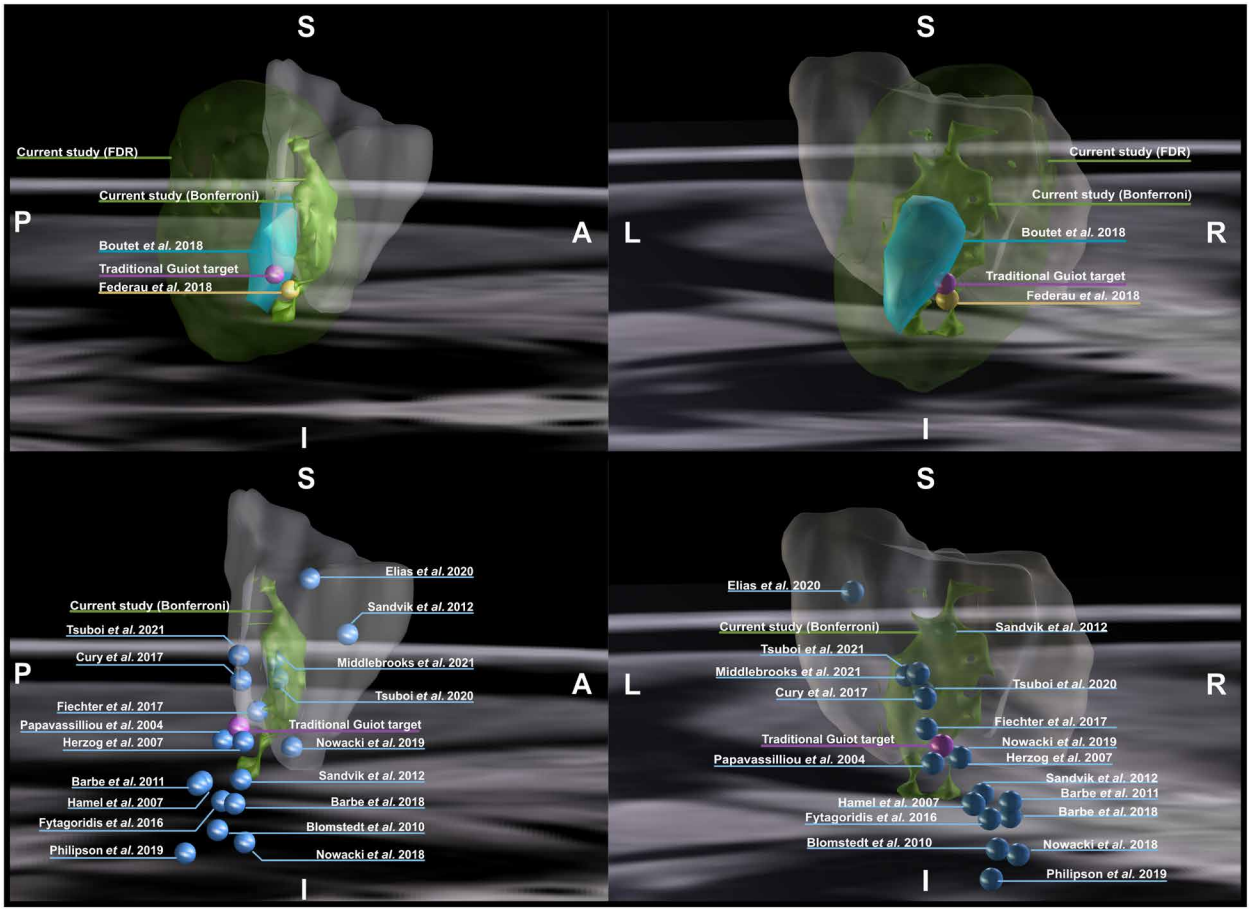

Fig. 7. Comparison with published results. Spatial relationships between our identified sweetspot and previously published optimal targets for MRgFUS thalamotomy in ET (top row) and spatial relationship of published DBS sweetspots. In the top row, our sweetspot after Bonferroni correction (green) and FDR correction (translucent green) and optimal FUS targets from Boutet *et al.* (*23*), retrieved from Lead-DBS software (blue), and Federau *et al.* (*22*) (yellow) are shown, and in the bottom row are published DBS sweetspots, with the traditional Guiot target (purple) and the Bonferroni-corrected sweetspot identified in the present study in views from the right (sagittal orientation, left) and from the back (coronal orientation, right) planes on a fast gray matter acquisition T1 inversion recovery brain scan in MNI space. The Vim (based on the DISTAL atlas) is shown in translucent white in all panels. Comparison includes studies (*22*), (*23*), (*26*), (*57*), and (*61-77*).

sourspot could also reflect contribution of proprioception loss. Critically, the sourspot for imbalance was the only one that partly overlapped with the sweetspot for tremor reduction. However, the two spots were not identical. Potentially, a differentiation may be possible in future research based on prospective studies and/or larger retrospective cohorts. Although only significant at the uncorrected level, we found that superomedial lesions were associated with dysarthria, which could represent lesion extension into the face/mouth/tongue area of the Vim (fig. S6). In line with these findings, Montgomery (*34*) has associated medial thalamic DBS stimulation with speech impairments. Alternatively, some reports have associated the occurrence of dysarthria with disruptions of passing pallidal fibers projecting into the ventral anterior and ventral lateral (VL) nuclei in a network connected with Broca's area or pallidal fibers projecting to medial VL in a network connected with primary motor cortex (*35*–*38*). Broadly, in our cohort, dysarthria may arise from sensory, motor, or mixed lesioning in oral regions, or potentially from higher-order motor coordination networks associated with the broader spectrum of dysarthria and speech apraxia. Further discrimination would require elaborate speech and language assessments that could specifically segregate both our hypotheses and results of dysarthria-related sourspots. Our results associated dysgeusia (at the uncorrected level) to more posterior lesions, likely extending into the VPL or VPM nuclei, as well as trigeminothalamic and medial lemniscal fibers that are thought to represent gustation. In line with this, De Vloo *et al.* (*39*) reported post-MRgFUS thalamotomy dysgeusia in a patient and found disruption of solitariothalamic gustatory fibers (medial border of the medial lemniscus). Carlson *et al.* (*40*) also reported that Vim-DBS leads causing dysgeusia were more posteriorly placed compared to leads that did not cause dysgeusia.

While a precisely placed lesion is important, lesion size is a similarly important factor. Lesions are thought to be represented by Wintermark zones 1 and 2, and findings on T2-weighted MRI have been correlated with histopathological findings (*29*, *41*–*43*). Prior reports have suggested that a minimum lesion volume of 40 mm^3 is required for tremor benefit (*44*, *45*). Boutet *et al.* (*23*) did not identify significant associations between lesion size and tremor outcomes. However, in their sample, lesions larger than 170 mm^3 were associated with higher risks of acute side effects. This association

Table 3. Coordinates of previously published tremor sweetspots in comparison to this study.

Study	Peak/Centroid	Coordinates (MNI space)			Coordinates (AC/PC space)		
		X (mm)	*Y* (mm)	*Z* (mm)	Lateral to MCP (mm)	Posterior to MCP (mm)	Superior to AC/PC line (mm)
FUS studies							
Current study	Peak	−14.72	−14.6	1.4	15.47 ± 1.27	3.23 ± 0.79	3.47 ± 0.61
	Centroid	−14.17	−17.42	0.38	14.75 ± 1.18	5.82 ± 0.75	2.44 ± 0.57
Boutet *et al.* (*23*)	Centroid	−15.09	−17.06	0.93	15.71 ± 1.23	5.51 ± 0.78	2.93 ± 0.60
Federau *et al.* (*22*)	Average	−13.78	−16.26	−2.89	14.3	4.5	0
DBS studies							
Papavassiliou *et al.* (*62*)		−14.5	−17.7		−2.8		
Hamel *et al.* (*63*)		−12.9	−18.6		−4.5	12.7 ± 1.4	7.0 ± 1.6	−1.5 ± 2.0
Herzog *et al.* (*64*)		−13.2	−16.8		−2.7	13	5.5	0
Blomstedt *et al.* (*65*)		−11.8	−17.9		−6.5	11.6 ± 1.8	6.3 ± 1.6	−3.0 ± 2.3
Barbe *et al.* (*66*)		−11.4	−18.8		−4.4	11.3 ± 1.6	7.2 ± 1.7	−1.4 ± 1.2
Sandvik *et al.* (*67*)		−13.1	−12.2		2.3	13 ± 1.4	1.8 ± 0.5	4.1 ± 0.3
Sandvik *et al.* (*67*)		−12.3	−16.9		−4.3	12.1 ± 1.4	5.5 ± 1.9	−1.2 ± 2.9
Fytagoridis *et al.* (*68*)		−12.1	−17.7		−5.2	11.9 ± 1.4	6.7 ± 1.5	−2.4 ± 2.0
Cury *et al.* (*69*)		−14.7	−16.9		−0.1	14.7 ± 2.2	6.7 ± 1.3	1.9 ± 2.5
Fiechter *et al.* (*70*)		−14.5	−16.17		−1.5	14.3 ± 1.6	5.0 ± 0.9	0.9 ± 1.2
Barbe *et al.* (*71*)		−11.2	−17.2		−5.2	11.0 ± 1.4	5.7 ± 1.4	−1.9 ± 0.6
Nowacki *et al.* (*72*)		−10.8	−16.7		−6.9	10.6 ± 0.8	5.2 ± 0.7	−3.2 ± 0.5
Nowacki *et al.* (*73*)		−13.0	−14.7		−2.9	12.8 ± 1.5	3.6 ± 1.0	0.0 ± 0.0
Philipson *et al.* (*74*)		−12.3	−19.3		−7.7	12.0	7.5	−4.0
Tsuboi *et al.* (*75*)		−15	−17		1			
Elias *et al.* (*57*)		−17.3	−13.9		4.2			
Tsuboi *et al.* (*76*)		−14.5	−15.3		0.0	14.3 ± 1.6	4.3 ± 1.5	−2.1 ± 2.3
Middlebrooks *et al.* (*77*)		−15.3	−15.5		0.8			

matches our results, by which larger lesion size was associated with the occurrence of side effects. Critically, lesions in our sample were larger overall, with a mean of 462.90 ± 190.15 mm^3 [versus an average of 181 mm^3 in Boutet *et al.* (*23*)]. In our sample, lesion size did associate with tremor improvements, when analyzed in isolation. However, when analyzed in a joint model with lesion location, as expressed by overlaps with the sweetspot (analyzed without circularity in a k-fold design), only lesion location, not lesion volume, explained significant amounts of variance in tremor outcomes.

Several limitations apply to the present study. First, our sample lacks complete CRST scores and quality-of-life data, which precludes more detailed conclusions about efficacy and comparison to other studies. Tremor outcomes and side effects were queried via telehealth in most cases, using a structured adverse events questionnaire that has not been validated for telehealth in a dedicated fashion. However, significant cross-validation results of our findings suggest internal integrity of our results. Potentially, adverse events could have been underrated because more accurate scales for ataxia were not performed and a high percent of individuals had side effects collected by telehealth. Side effect sourspot calculations were only conducted in the discovery cohort because data were only available for this cohort. Most of our patients had excellent clinical outcomes, with 64.5% (98 of 152) patients achieving 100% improvement in their overall FTM score at 1-year postprocedure. This, in addition to few negative controls (only 6 patients had 0% improvement in their overall FTM score at 1 year), the large size of lesions, and the binary nature of the lesion segmentations, rendered sweetspot analysis nontrivial and might have biased our results. To this end, we consulted with statisticians and experts (T.A.D. and G.M.M.) in the field of sweetspot mapping and carefully investigated results in comparison to frequency maps by top-responding and poor-responding patients, in relation to poorest responding and retreatment cases (*31*). Despite the amount of thought and care that went into our analysis, results are unable to define the final volume needed to lesion for optimal tremor results without side effects. Critically, sweet- and sourspot results (and analogous tract findings) should be seen as the regions and tracts that best differentiate top- from poor-responding cases. Hence, while they may form a conditio sine qua non, they do not represent the areas/tracts that need to be exclusively lesioned. To make further advances in this direction, future studies could incorporate segmentations of Wintermark zones 1 and 2 separately to be able to model lesions in a more probabilistic sense in association with outcomes, as is frequently done in DBS (*46*). Lesions were defined based on MRI scans acquired on the first postoperative day, which does not allow insights of lesion evolution over time. However, our recent work showed that even after 3 months, lesions were

only detectable on thin-cut T2-weighted MRI in 55% of cases (*29*), which would not allow sweetspot mapping in an unbiased way.

In conclusion, we identified a set of optimal sites and fiber tracts, as well as locations and tracts of avoidance based on the largest cohort of focused ultrasound cases for treatment of ET published to date. Our results may help guide targeting in future cases to maximize clinical outcomes and reduce the frequency of side effects in MRgFUS for ET.

MATERIALS AND METHODS

Patient population

The study comprised three cohorts of patients that underwent MRgFUS thalamotomy at BWH in Boston ($n = 302$) or at TWH or SHSC in Toronto and were divided into a BWH discovery cohort ($n = 200$), as well as a BWH validation cohort ($n = 102$) and a Toronto validation cohort ($n = 49$). Models were calculated on the discovery cohort and validated by estimating variance in lesions from the two independent validation cohorts.

BWH Discovery and Validation Cohort (total $n = 302$): All patients with medically refractory ET who underwent unilateral MRgFUS Vim thalamotomy at BWH between June 2016 and June 2022 were included in this cohort. Ten patients did not return for imaging on postoperative day 1 and were thus excluded. Patients who did not return for both 3-month and 1-year follow-up were also excluded. Six patients had recurrence of tremor and underwent a repeat procedure, yielding a final total of 302 thalamotomy cases. These were divided into an initial discovery cohort ($n = 200$) and a validation cohort ($n = 102$). A skull-density ratio (SDR) of at least 0.35 was the minimum requirement for treatment consideration.

Toronto Multi-Site Validation Cohort (total $n = 49$): Retrospective data collection of patients with medically refractory ET who underwent unilateral MRgFUS Vim thalamotomy at TWH and SHSC between May 2012 and February 2016 was performed for this cohort. Patients with any SDR were included. Patients were excluded if they lacked 3-month and 1 year tremor scores.

This study was approved by the respective institutional review boards [IRB protocol #2020P000476, IRB protocol #19-6194 (TWH) and #1822 (SHSC)] and conducted in line with the Declaration of Helsinki and Good Clinical Practice guidelines. All participants gave written informed consent before study participation.

Procedure

The detailed procedural workflow at our institution has been previously published (*30*, *47*). In brief, preoperative computed tomography (CT) scans were obtained to assess each patient's SDR. On the day of surgery, the patient's head was completely shaved, and a modified Cosman-Roberts-Wells frame (Radionics Inc.) was applied under local anesthesia. A waterproof silicone membrane was stretched over the patient's head before placement in a 3-T MRI scanner (GE Medical Systems) and connected to the ExAblate 4000 MRgFUS transducer (InSightec Inc., Israel). Degassed and cooled water was filled in the silicone membrane. Preoperative CT and MRI scans were fused to account for skull aberrations, and calcifications were excluded from ultrasound exposure. Initial baseline MRI scans were obtained for targeting based on standardized atlas-based stereotactic coordinates of the Vim (25% of AC-PC distance anterior to PC, 13 to 14 mm lateral to midline or 11 mm lateral from the wall of the third ventricle, and 1.5 to 2 mm superior to the plane of AC-PC). Targeting was refined on an individual basis with direct visualization. Subclinical test sonications at low energy were then carried out to confirm targeting and transient clinical symptomatic improvement between each test sonication. Following confirmation of the final desired target, high-powered treatment sonications were delivered sequentially with maximum temperature between 55° and 60°C. After initial successful first treatment sonication, we moved superiorly by 1 to 2 mm for the next sonication. Real-time MR thermometry was used to monitor lesion location and temperature achieved. Clinical testing was conducted after each sonication to confirm tremor improvement and avoidance of side effects.

Clinical outcomes

Preoperative baseline and postoperative follow-up tremor assessments were performed using subitems from part A of the Fahn-Tolosa-Marin (FTM) tremor clinical rating scale (*48*). Namely, composite scores of the following categories with 0 to 4 points (no tremor—0; slight tremor—1; moderate tremor—2; marked tremor—3; severe tremor—4) were assigned to each category, yielding a maximum total score of 20: vocal tremor, head tremor, resting tremor of the affected limb, intention tremor of the affected limb, and postural tremor of the affected limb. We also report intention and posture FTM scores, which combines 0- to 4-point scores for intention and postural tremors of the affected limb, yielding a maximum total score of 8. For the purpose of this manuscript, these subitems of the score will be referred to as FTM tremor score (total) or (intention/postural), respectively. Clinical follow-up was conducted on postoperative day 1, as well as at 3 months and 1 year. Percent tremor improvement at each time point was calculated relative to the baseline tremor score. Side effects were documented at every postoperative visit, which included weakness, sensory deficits (paresthesias and/or numbness), dysarthria, dysgeusia (except on day 1), and gait imbalance; severity was additionally graded based on the Clavien-Dindo criteria (*25*). All preoperative and postoperative day 1 clinical assessments were conducted in-person. All other postoperative follow-up assessments were performed either in-person or via telemedicine visits. The majority of patients were evaluated by telehealth at 3 and 12 months and asked to rate their tremor control as a percentage improved from preoperative baseline. They were administered the structured adverse events questionnaire and asked for their subjective response consistent with the Clavien-Dindo criteria. Follow-up numbers at each time point varied due to individual patient availability and/or ability to return to clinic.

Lesion segmentation and volume analysis

All patients underwent postoperative MRI on the day following the procedure. Lesions were manually segmented on thin-cut (2 mm) T2 axial images in patient native space using a predefined semiautomated workflow integrated in the Structured Planning and Implementation of New Experiments (SPINE) web-based platform (*49*). Manual segmentations of the lesions were facilitated by limiting them to a preset image intensity range, defined by histogram analysis of a region sampled at the interface between lesions and surrounding tissue. Segmentations were performed by two separate individuals and interrater agreements were assessed. Lesions were defined as Wintermark zones 1 and 2, which represent central necrosis and cytotoxic edema, respectively. Wintermark zone 3 represents vasogenic edema and was not included in the analysis (*41*, *42*).

Lesion volumes were calculated from the three-dimensional (3D) lesion segmentations of Wintermark zones 1 and 2.

Volume registration

Using Lead-DBS v3.0, MRI images were linearly coregistered using SPM 12 (www.fil.ion.ucl.ac.uk/spm/software/spm12/) (*50, 51*). Coregistered images were then nonlinearly transformed to ICBM 2009b NLIN asymmetric standard MNI space using the Symmetric Normalization (SyN) Diffeomorphic Mapping algorithm as implemented in Advanced Normalization Tools (ANTs; http://stnava.github.io/ANTs/) (*52*). This procedure was carried out using a multispectral implementation and normalization parameters that had been optimized for subcortical registrations as implemented in the "Effective: Low Variance + subcortical refinement" setting in Lead-DBS (*53*). The resulting patient-specific transformations were applied to each patient's segmented lesion to map to standard space. Normalized lesions of patients who underwent right-sided thalamotomy ($n = 37$) were flipped to the left hemisphere using Lead-DBS.

Sweetspot and sourspot analyses

The Sweetspot Explorer tool within Lead-DBS v3.0 was used to investigate sites corresponding to optimal outcomes (i.e., "sweetspots") and side effects (i.e., "sourspots") (*50*). Here, we based methodological choices on experience obtained in the DBS field, where binary stimulation volumes have been used to map optimal improvements (*54, 55*). While numerous strategies for sweetspot mapping have been introduced over the years, a recent comparative study in DBS favored a specific strategy that we adopted here (*31*). Namely, voxels covered by at least 20% of lesions were included in the analysis. Then, a voxel-wise Wilcoxon-signed rank test against the average percent FTM tremor score improvement (which was 86.0% at 1 year in our cohort) was performed to compute the tremor sweetspot (*56, 57*). In other words, we aimed to identify voxels whose lesion overlap was associated with better than average clinical outcome. Because MNI coordinates are substantially different to stereotactic coordinates, sweetspot coordinates were converted to AC-PC coordinates in probabilistic fashion for broader applicability (*26*). Similar to the sweetspot strategy, we mapped the occurrence of side effects to anatomical regions. Because side effects were measured in binary fashion, here, we used voxel-wise proportion tests that could outline sourspots for each side effect. A P value of less than 0.05 was considered statistically significant after correction for multiple comparisons using FDR and/or Bonferroni methods. Consistency of sweet- and sourspot results were probed by subjecting them to 10-fold cross-validation tests as described before (*46, 58*). These results can be seen as a measure of how well results would generalize to unseen data, i.e., how well the sweet- and sourspot models could be used to estimate improvements and occurrence of side effects in unseen (independent) patients, respectively. Univariate analyses determining associations between lesion size and each side effect were performed using two-sided t tests.

Validation of sweetspot results using independent cohorts

In the same fashion as cross-validation analyses, we validated the sweetspot model using unseen independent out-of-sample data from three hospitals. This was done by multiplying the sweetspot (thresholded at FDR significance) with novel (binary) lesions and averaging voxels of overlap. This coefficient (weighted average overlap) was then correlated with clinical improvements empirically collected in these cohorts with the idea that high overlap scores would lead to high tremor improvements (*46*). The same subscores of the FTM tremor clinical rating scale were used across the three hospitals to ensure direct comparison and accurate validation across the cohorts.

Fiber tract analysis

As a second step, we carried out an adaptation of DBS fiber filtering (*24*). This technique statistically associates specific streamlines from a given set with clinical improvements (or the occurrence of side effects). These types of analyses have been facilitated with the introduction of the Fiber Filtering Explorer in Lead-DBS v3.0, which was used here (*50*). Analogous to the sweetspot strategy, fibers were considered if they were covered by at least 20% of lesions. For each streamline, two-sample t tests were calculated that compared percent FTM tremor scores between patients in which the streamline was covered by the lesion and the ones that were not. The resulting t score was assigned to the respective streamline (*59*). Similarly, proportion tests were carried out for side effects (binary outcomes) to determine white matter fibers statistically associated with the occurrence of specific side effects. This procedure was repeated for each streamline implemented in the DBS Tractography Atlas v2 or the Basal Ganglia Pathway Atlas (*18, 60*). These atlases consist of the most detailed 3D streamline atlases of the thalamic region available to date. After tracts that were associated with improvements or side effects were identified, they were subjected to 10-fold cross-validation and split half validation tests to assess robustness. Similar to sweetspot results, this analysis can be seen as a measure of how well tract findings would generalize to unseen data, i.e., how well the sweet and sour tract models could be used to correlate improvements and occurrence of side effects in unseen (independent) patients, respectively.

Supplementary Materials

This PDF file includes:

Figs. S1 to S6
Table S1

REFERENCES AND NOTES

1. E. D. Louis, Treatment of medically refractory essential tremor. *N. Engl. J. Med.* **375**, 792–793 (2016).
2. E. D. Louis, J. J. Ferreira, How common is the most common adult movement disorder? Update on the worldwide prevalence of essential tremor. *Mov. Disord.* **25**, 534–541 (2010).
3. G. Deuschl, J. Raethjen, H. Hellriegel, R. Elble, Treatment of patients with essential tremor. *Lancet Neurol.* **10**, 148–161 (2011).
4. W. J. Elias, N. Lipsman, W. G. Ondo, P. Ghanouni, Y. G. Kim, W. Lee, M. Schwartz, K. Hynynen, A. M. Lozano, B. B. Shah, D. Huss, R. F. Dallapiazza, R. Gwinn, J. Witt, S. Ro, H. M. Eisenberg, P. S. Fishman, D. Gandhi, C. H. Halpern, R. Chuang, K. Butts Pauly, T. S. Tierney, M. T. Hayes, G. R. Cosgrove, T. Yamaguchi, K. Abe, T. Taira, J. W. Chang, A randomized trial of focused ultrasound thalamotomy for essential tremor. *N. Engl. J. Med.* **375**, 730–739 (2016).
5. G. R. Cosgrove, N. Lipsman, A. M. Lozano, J. W. Chang, C. Halpern, P. Ghanouni, H. Eisenberg, P. Fishman, T. Taira, M. L. Schwartz, N. McDannold, M. Hayes, S. Ro, B. Shah, R. Gwinn, V. E. Santini, K. Hynynen, W. J. Elias, Magnetic resonance imaging-guided focused ultrasound thalamotomy for essential tremor: 5-year follow-up results. *J. Neurosurg.* **138**, 1028–1033 (2023).
6. F. Sammartino, V. Krishna, N. K. K. King, A. M. Lozano, M. L. Schwartz, Y. Huang, M. Hodaie, Tractography-based ventral intermediate nucleus targeting: Novel methodology and intraoperative validation. *Mov. Disord.* **31**, 1217–1225 (2016).

7. A. Abosch, E. Yacoub, K. Ugurbil, N. Harel, An assessment of current brain targets for deep brain stimulation surgery with susceptibility-weighted imaging at 7 tesla. *Neurosurgery* **67**, 1745–1756 (2010).
8. F. Vassal, J. Coste, P. Derost, V. Mendes, J. Gabrillargues, C. Nuti, F. Durif, J.-J. Lemaire, Direct stereotactic targeting of the ventrointermediate nucleus of the thalamus based on anatomic 1.5-T MRI mapping with a white matter attenuated inversion recovery (WAIR) sequence. *Brain Stimul.* **5**, 625–633 (2012).
9. A. Sudhyadhom, I. U. Haq, K. D. Foote, M. S. Okun, F. J. Bova, A high resolution and high contrast MRI for differentiation of subcortical structures for DBS targeting: The Fast Gray Matter Acquisition T1 Inversion Recovery (FGATIR). *Neuroimage* **47** (Suppl. 2), T44–T52 (2009).
10. J. L. Chazen, H. Sarva, P. E. Stieg, R. J. Min, D. J. Ballon, K. O. Pryor, P. M. Riegelhaupt, M. G. Kaplitt, Clinical improvement associated with targeted interruption of the cerebellothalamic tract following MR-guided focused ultrasound for essential tremor. *J. Neurosurg.* **129**, 315–323 (2018).
11. F. Bruno, A. Catalucci, M. Varrassi, F. Arrigoni, P. Sucapane, D. Cerone, F. Pistoia, S. Torlone, E. Tommasino, L. De Santis, A. Barile, A. Ricci, C. Marini, A. Splendiani, C. Masciocchi, Comparative evaluation of tractography-based direct targeting and atlas-based indirect targeting of the ventral intermediate (Vim) nucleus in MRgFUS thalamotomy. *Sci. Rep.* **11**, 13538 (2021).
12. V. T. Lehman, K. H. Lee, B. T. Klassen, D. J. Blezek, A. Goyal, B. R. Shah, K. R. Gorny, J. Huston, T. J. Kaufmann, MRI and tractography techniques to localize the ventral intermediate nucleus and dentatorubrothalamic tract for deep brain stimulation and MR-guided focused ultrasound: A narrative review and update. *Neurosurg. Focus* **49**, E8 (2020).
13. T. R. Miller, J. Zhuo, H. M. Eisenberg, P. S. Fishman, E. R. Melhem, R. Gullapalli, D. Gandhi, Targeting of the dentato-rubro-thalamic tract for MR-guided focused ultrasound treatment of essential tremor. *Neuroradiol. J.* **32**, 401–407 (2019).
14. M. A. Morrison, A. T. Lee, A. J. Martin, C. Dietiker, E. G. Brown, D. D. Wang, DBS targeting for essential tremor using intersectional dentato-rubro-thalamic tractography and direct proton density visualization of the VIM: Technical note on 2 cases. *J. Neurosurg.* **135**, 806–814 (2021).
15. A. I. Yang, D. Parker, A. A. Vijayakumari, A. G. Ramayya, M. P. Donley-Fletcher, D. Aunapu, R. L. Wolf, G. H. Baltuch, R. Verma, Tractography-based surgical targeting for thalamic deep brain stimulation: A comparison of probabilistic vs deterministic fiber tracking of the dentato-rubro-thalamic tract. *Neurosurgery* **90**, 419–425 (2022).
16. M. V. Petersen, T. E. Lund, N. Sunde, J. Frandsen, F. Rosendal, N. Juul, K. Østergaard, Probabilistic versus deterministic tractography for delineation of the cortico-subthalamic hyperdirect pathway in patients with Parkinson disease selected for deep brain stimulation. *J. Neurosurg.* **126**, 1657–1668 (2017).
17. A. Jakab, B. Werner, M. Piccirelli, K. Kovács, E. Martin, J. S. Thornton, T. Yousry, G. Székely, R. O'Gorman Tuura, Feasibility of diffusion tractography for the reconstruction of intra-thalamic and cerebello-thalamic targets for functional neurosurgery: A multi-vendor pilot study in four subjects. *Front. Neuroanat.* **10**, 76 (2016).
18. M. V. Petersen, J. Mlakar, S. N. Haber, M. Parent, Y. Smith, P. L. Strick, M. A. Griswold, C. C. McIntyre, Holographic reconstruction of axonal pathways in the human brain. *Neuron* **104**, 1056–1064.e3 (2019).
19. A. Horn, S. Ewert, E. J. L. Alho, M. Axer, H. Heinsen, E. T. Fonoff, J. R. Polimeni, T. M. Herrington, Teaching neuroimages: In-vivo visualization of Edinger's comb and Wilson's pencils. *Neurology* **92**, e1663–e1664 (2019).
20. E. J. L. Alho, A. T. D. L. Alho, A. Horn, M. da Graça M Martin, B. L. Edlow, B. Fischl, J. Nagy, E. T. Fonoff, C. Hamani, H. Heinsen, The Ansa Subthalamica: A neglected fiber tract. *Mov. Disord.* **35**, 75–80 (2020).
21. K. Hynynen, N. I. Vykhodtseva, A. H. Chung, V. Sorrentino, V. Colucci, F. A. Jolesz, Thermal effects of focused ultrasound on the brain: Determination with MR imaging. *Radiology* **204**, 247–253 (1997).
22. C. Federau, M. Goubran, J. Rosenberg, J. Henderson, C. H. Halpern, V. Santini, M. Wintermark, K. Butts Pauly, P. Ghanouni, Transcranial MRI-guided high-intensity focused ultrasound for treatment of essential tremor: A pilot study on the correlation between lesion size, lesion location, thermal dose, and clinical outcome. *J. Magn. Reson. Imaging* **48**, 58–65 (2018).
23. A. Boutet, M. Ranjan, J. Zhong, J. Germann, D. Xu, M. L. Schwartz, N. Lipsman, K. Hynynen, G. A. Devenyi, M. Chakravarty, E. Hlasny, M. Llinas, C. S. Lozano, G. J. B. Elias, J. Chan, A. Coblentz, A. Fasano, W. Kucharczyk, M. Hodaie, A. M. Lozano, Focused ultrasound thalamotomy location determines clinical benefits in patients with essential tremor. *Brain* **141**, 3405–3414 (2018).
24. J. C. Baldermann, C. Melzer, A. Zapf, S. Kohl, L. Timmermann, M. Tittgemeyer, D. Huys, V. Visser-Vandewalle, A. A. Kühn, A. Horn, J. Kuhn, Connectivity profile predictive of effective deep brain stimulation in obsessive-compulsive disorder. *Biol. Psychiatry* **85**, 735–743 (2019).
25. D. Dindo, N. Demartines, P.-A. Clavien, Classification of surgical complications: A new proposal with evaluation in a cohort of 6336 patients and results of a survey. *Ann. Surg.* **240**, 205–213 (2004).
26. A. Horn, A. A. Kühn, A. Merkl, L. Shih, R. Alterman, M. Fox, Probabilistic conversion of neurosurgical DBS electrode coordinates into MNI space. *Neuroimage* **150**, 395–404 (2017).
27. C. Neudorfer, K. Kultas-Ilinsky, I. Ilinsky, S. Paschen, A.-K. Helmers, G. R. Cosgrove, R. M. Richardson, A. Horn, G. Deuschl, The role of the motor thalamus in deep brain stimulation for essential tremor. *Neurotherapeutics* **21**, e00313 (2024).
28. C. Neudorfer, D. Kroneberg, B. Al-Fatly, L. Goede, D. Kübler, K. Faust, U. Rienen, A. Tietze, T. Picht, T. M. Herrington, E. H. Middlebrooks, A. Kühn, G.-H. Schneider, A. Horn, Personalizing deep brain stimulation using advanced imaging sequences. *Ann. Neurol.* **91**, 613–628 (2022).
29. S. E. Blitz, M. M. J. Chua, P. Ng, D. J. Segar, R. Jha, N. J. McDannold, M. N. DeSalvo, J. D. Rolston, G. R. Cosgrove, Longitudinal MR imaging after unilateral MR-guided focused ultrasound thalamotomy: Clinical and radiological correlation. *Front. Neurol.* **14**, 1272425 (2023).
30. D. J. Segar, A. M. Lak, S. Lee, M. Harary, V. Chavakula, P. Lauro, N. McDannold, J. White, G. R. Cosgrove, Lesion location and lesion creation affect outcomes after focused ultrasound thalamotomy. *Brain* **144**, 3089–3100 (2021).
31. T. A. Dembek, J. C. Baldermann, J.-N. Petry-Schmelzer, H. Jergas, H. Treuer, V. Visser-Vandewalle, H. S. Dafsari, M. T. Barbe, Sweetspot mapping in deep brain stimulation: Strengths and limitations of current approaches. *Neuromodulation* **25**, 877–887 (2022).
32. T. Sprenger, C. L. Seifert, M. Valet, A. P. Andreou, A. Foerschler, C. Zimmer, D. L. Collins, P. J. Goadsby, T. R. Tölle, M. M. Chakravarty, Assessing the risk of central post-stroke pain of thalamic origin by lesion mapping. *Brain* **135**, 2536–2545 (2012).
33. M. Paff, A. Boutet, J. Germann, G. J. B. Elias, C. T. Chow, A. Loh, W. Kucharczyk, A. Fasano, M. L. Schwartz, A. M. Lozano, Focused ultrasound thalamotomy sensory side effects follow the thalamic structural homunculus. *Neurol. Clin. Pract.* **11**, e497–e503 (2021).
34. E. B. Montgomery Jr., *Deep Brain Stimulation Programming: Principles and Practice* (Oxford Univ. Press, 2010).
35. G. A. Ojemann, A. A. Ward Jr., Speech representation in ventrolateral thalamus. *Brain* **94**, 669–680 (1971).
36. F. Lhermitte, Language disorders and their relationship to thalamic lesions. *Adv. Neurol.* **42**, 99–113 (1984).
37. J. D. Schmahmann, Vascular syndromes of the thalamus. *Stroke* **34**, 2264–2278 (2003).
38. A. V. Varma-Doyle, N. R. Villemarette-Pittman, B. J. Copeland, Hemi-parkinsonism and return of essential tremors after MRgFUS thalamotomy: Case report and review of procedural complications affecting ventral thalamic nuclei. *eNeurologicalSci* **23**, 100339 (2021).
39. P. De Vloo, A. Boutet, G. J. B. Elias, R. M. Gramer, S. E. Joel, M. Llinas, W. Kucharczyk, A. Fasano, C. Hamani, A. M. Lozano, Dysgeusia induced and resolved by focused ultrasound thalamotomy: Case report. *J. Neurosurg.* **136**, 215–220 (2022).
40. J. D. Carlson, K. E. McLeod, J. B. Mark, P. S. McLeod, B. A. Bremer, Dysgeusia in deep brain stimulation for essential tremor. *J. Clin. Neurosci.* **50**, 242–246 (2018).
41. M. Wintermark, J. Druzgal, D. S. Huss, M. A. Khaled, S. Monteith, P. Raghavan, T. Huerta, L. C. Schweickert, B. Burkholder, J. J. Loomba, E. Zadicario, Y. Qiao, B. Shah, J. Snell, M. Eames, R. Frysinger, N. Kassell, W. J. Elias, Imaging findings in MR imaging-guided focused ultrasound treatment for patients with essential tremor. *AJNR Am. J. Neuroradiol.* **35**, 891–896 (2014).
42. S. E. Blitz, M. Torre, M. M. J. Chua, S. L. Christie, N. J. McDannold, G. R. Cosgrove, Focused ultrasound thalamotomy: Correlation of postoperative imaging with neuropathological findings. *Stereotact. Funct. Neurosurg.* **101**, 60–67 (2023).
43. S. Koga, M. Ishaque, W. Jeffrey Elias, B. B. Shah, A. Murakami, D. W. Dickson, Neuropathology of Parkinson's disease after focused ultrasound thalamotomy. *NPJ Parkinsons Dis.* **8**, 59 (2022).
44. T. Hirai, M. Miyazaki, H. Nakajima, T. Shibazaki, C. Ohye, The correlation between tremor characteristics and the predicted volume of effective lesions in stereotaxic nucleus ventralis intermedius thalamotomy. *Brain* **106** (Pt. 4), 1001–1018 (1983).
45. Y. Nagaseki, T. Shibazaki, T. Hirai, Y. Kawashima, M. Hirato, H. Wada, M. Miyazaki, C. Ohye, Long-term follow-up results of selective VIM-thalamotomy. *J. Neurosurg.* **65**, 296–302 (1986).
46. A. Horn, M. M. Reich, S. Ewert, N. Li, B. Al-Fatly, F. Lange, J. Roothans, S. Oxenford, I. Horn, S. Paschen, J. Runge, F. Wodarg, K. Witt, R. C. Nickl, M. Wittstock, G.-H. Schneider, P. Mahlknecht, W. Poewe, W. Eisner, A.-K. Helmers, C. Matthies, J. K. Krauss, G. Deuschl, J. Volkmann, A. A. Kühn, Optimal deep brain stimulation sites and networks for cervical vs. generalized dystonia. *Proc. Natl. Acad. Sci. U.S.A.* **119**, e2114985119 (2022).
47. M. Harary, W. I. Essayed, P. A. Valdes, N. McDannold, G. R. Cosgrove, Volumetric analysis of magnetic resonance-guided focused ultrasound thalamotomy lesions. *Neurosurg. Focus* **44**, E6 (2018).
48. S. Fahn, E. Tolosa, C. Marín, "Clinical rating scale for tremor," in *Parkinson's Disease and Movement Disorders* (Williams and Wilkins, 1993), pp. 271–280.
49. M. Deol, M. Palotai, A. M. Pinzon, A. Marciniak, G. Bliault, E. Covert, A. Aizer, J. P. Guenette, M. N. Desalvo, X. T. Li, A. Thomas, N.-A. Tran, A. Jacobson, R. Huang, C. R. G. Guttmann,

Identification and characterization of leptomeningeal metastases using SPINE, a web-based collaborative platform. *J. Neuroimaging* **31**, 324–333 (2021).
50. C. Neudorfer, K. Butenko, S. Oxenford, N. Rajamani, J. Achtzehn, L. Goede, B. Hollunder, A. S. Ríos, L. Hart, J. Tasserie, K. B. Fernando, T. A. K. Nguyen, B. Al-Fatly, M. Vissani, M. Fox, R. M. Richardson, U. van Rienen, A. A. Kühn, A. D. Husch, E. Opri, T. Dembek, N. Li, A. Horn, Lead-DBS v3.0: Mapping deep brain stimulation effects to local anatomy and global networks. *Neuroimage* **268**, 119862 (2023).
51. A. Horn, A. A. Kühn, Lead-DBS: A toolbox for deep brain stimulation electrode localizations and visualizations. *Neuroimage* **107**, 127–135 (2015).
52. B. B. Avants, N. J. Tustison, G. Song, P. A. Cook, A. Klein, J. C. Gee, A reproducible evaluation of ANTs similarity metric performance in brain image registration. *Neuroimage* **54**, 2033–2044 (2011).
53. S. Ewert, A. Horn, F. Finkel, N. Li, A. A. Kühn, T. M. Herrington, Optimization and comparative evaluation of nonlinear deformation algorithms for atlas-based segmentation of DBS target nuclei. *Neuroimage* **184**, 586–598 (2019).
54. A. Horn, The impact of modern-day neuroimaging on the field of deep brain stimulation. *Curr. Opin. Neurol.* **32**, 511–520 (2019).
55. C. R. Butson, S. E. Cooper, J. M. Henderson, B. Wolgamuth, C. C. McIntyre, Probabilistic analysis of activation volumes generated during deep brain stimulation. *Neuroimage* **54**, 2096–2104 (2011).
56. T. A. Dembek, J. Roediger, A. Horn, P. Reker, C. Oehrn, H. S. Dafsari, N. Li, A. A. Kühn, G. R. Fink, V. Visser-Vandewalle, M. T. Barbe, L. Timmermann, Probabilistic sweet spots predict motor outcome for deep brain stimulation in Parkinson disease. *Ann. Neurol.* **86**, 527–538 (2019).
57. G. J. B. Elias, A. Boutet, S. E. Joel, J. Germann, D. Gwun, C. Neudorfer, R. M. Gramer, M. Algarni, V. Paramanandam, S. Prasad, M. E. Beyn, A. Horn, R. Madhavan, M. Ranjan, C. S. Lozano, A. A. Kühn, J. Ashe, W. Kucharczyk, R. P. Munhoz, P. Giacobbe, S. H. Kennedy, D. B. Woodside, S. K. Kalia, A. Fasano, M. Hodaie, A. M. Lozano, Probabilistic mapping of deep brain stimulation: Insights from 15 years of therapy. *Ann. Neurol.* **89**, 426–443 (2021).
58. A. S. Ríos, S. Oxenford, C. Neudorfer, K. Butenko, N. Li, N. Rajamani, A. Boutet, G. J. B. Elias, J. Germann, A. Loh, W. Deeb, F. Wang, K. Setsompop, B. Salvato, L. B. de Almeida, K. D. Foote, R. Amaral, P. B. Rosenberg, D. F. Tang-Wai, D. A. Wolk, A. D. Burke, S. Salloway, M. N. Sabbagh, M. M. Chakravarty, G. S. Smith, C. G. Lyketsos, M. S. Okun, W. S. Anderson, Z. Mari, F. A. Ponce, A. M. Lozano, A. Horn, Optimal deep brain stimulation sites and networks for stimulation of the fornix in Alzheimer's disease. *Nat. Commun.* **13**, 7707 (2022).
59. N. Li, J. C. Baldermann, A. Kibleur, S. Treu, H. Akram, G. J. B. Elias, A. Boutet, A. M. Lozano, B. Al-Fatly, B. Strange, J. A. Barcia, L. Zrinzo, E. Joyce, S. Chabardes, V. Visser-Vandewalle, M. Polosan, J. Kuhn, A. A. Kühn, A. Horn, A unified connectomic target for deep brain stimulation in obsessive-compulsive disorder. *Nat. Commun.* **11**, 3364 (2020).
60. E. H. Middlebrooks, R. A. Domingo, T. Vivas-Buitrago, L. Okromelidze, T. Tsuboi, J. K. Wong, R. S. Eisinger, L. Almeida, M. R. Burns, A. Horn, R. J. Uitti, R. E. Wharen Jr., V. M. Holanda, S. S. Grewal, Neuroimaging advances in deep brain stimulation: Review of indications, anatomy, and brain connectomics. *AJNR Am. J. Neuroradiol.* **41**, 1558–1568 (2020).
61. M. M. Chakravarty, G. Bertrand, C. P. Hodge, A. F. Sadikot, D. L. Collins, The creation of a brain atlas for image guided neurosurgery using serial histological data. *Neuroimage* **30**, 359–376 (2006).
62. E. Papavassiliou, G. Rau, S. Heath, A. Abosch, N. M. Barbaro, P. S. Larson, K. Lamborn, P. A. Starr, Thalamic deep brain stimulation for essential tremor: Relation of lead location to outcome. *Neurosurgery* **54**, 1120–1130 (2004).
63. W. Hamel, J. Herzog, F. Kopper, M. Pinsker, D. Weinert, D. Müller, P. Krack, G. Deuschl, H. M. Mehdorn, Deep brain stimulation in the subthalamic area is more effective than nucleus ventralis intermedius stimulation for bilateral intention tremor. *Acta Neurochir.* **149**, 749–758 (2007).
64. J. Herzog, W. Hamel, R. Wenzelburger, M. Pötter, M. O. Pinsker, J. Bartussek, A. Morsnowski, F. Steigerwald, G. Deuschl, J. Volkmann, Kinematic analysis of thalamic versus subthalamic neurostimulation in postural and intention tremor. *Brain* **130**, 1608–1625 (2007).
65. P. Blomstedt, U. Sandvik, S. Tisch, Deep brain stimulation in the posterior subthalamic area in the treatment of essential tremor. *Mov. Disord.* **25**, 1350–1356 (2010).
66. M. T. Barbe, L. Liebhart, M. Runge, J. Deyng, E. Florin, L. Wojtecki, A. Schnitzler, N. Allert, V. Sturm, G. R. Fink, M. Maarouf, L. Timmermann, Deep brain stimulation of the ventral intermediate nucleus in patients with essential tremor: Stimulation below intercommissural line is more efficient but equally effective as stimulation above. *Exp. Neurol.* **230**, 131–137 (2011).
67. U. Sandvik, L.-O. Koskinen, A. Lundquist, P. Blomstedt, Thalamic and subthalamic deep brain stimulation for essential tremor: Where is the optimal target? *Neurosurgery* **70**, 840–846 (2012).
68. A. Fytagoridis, M. Åström, J. Samuelsson, P. Blomstedt, Deep brain stimulation of the caudal zona incerta: Tremor control in relation to the location of stimulation fields. *Stereotact. Funct. Neurosurg.* **94**, 363–370 (2017).
69. R. G. Cury, V. Fraix, A. Castrioto, M. A. Pérez Fernández, P. Krack, S. Chabardes, E. Seigneuret, E. J. L. Alho, A.-L. Benabid, E. Moro, Thalamic deep brain stimulation for tremor in Parkinson disease, essential tremor, and dystonia. *Neurology* **89**, 1416–1423 (2017).
70. M. Fiechter, A. Nowacki, M. F. Oertel, J. Fichtner, I. Debove, M. L. Lachenmayer, R. Wiest, C. L. Bassetti, A. Raabe, A. Kaelin-Lang, M. W. Schüpbach, C. Pollo, Deep brain stimulation for tremor: Is there a common structure? *Stereotact. Funct. Neurosurg.* **95**, 243–250 (2017).
71. M. T. Barbe, P. Reker, S. Hamacher, J. Franklin, D. Kraus, T. A. Dembek, J. Becker, J. K. Steffen, N. Allert, J. Wirths, H. S. Dafsari, J. Voges, G. R. Fink, V. Visser-Vandewalle, L. Timmermann, DBS of the PSA and the VIM in essential tremor: A randomized, double-blind, crossover trial. *Neurology* **91**, e543–e550 (2018).
72. A. Nowacki, I. Debove, F. Rossi, J. A. Schlaeppi, K. Petermann, R. Wiest, M. Schüpbach, C. Pollo, Targeting the posterior subthalamic area for essential tremor: Proposal for MRI-based anatomical landmarks. *J. Neurosurg.* **131**, 820–827 (2019).
73. A. Nowacki, M. Bogdanovic, N. Sarangmat, J. Fitzgerald, A. Green, T. Z. Aziz, Revisiting the rules for anatomical targeting of ventralis intermediate nucleus. *J. Clin. Neurosci.* **68**, 97–100 (2019).
74. J. Philipson, P. Blomstedt, M. Hariz, M. Jahanshahi, Deep brain stimulation in the caudal zona incerta in patients with essential tremor: Effects on cognition 1 year after surgery. *J. Neurosurg.* **134**, 208–215 (2021).
75. T. Tsuboi, Z. Jabarkheel, P. R. Zeilman, M. J. Barabas, K. D. Foote, M. S. Okun, A. Wagle Shukla, Longitudinal follow-up with VIM thalamic deep brain stimulation for dystonic or essential tremor. *Neurology* **94**, e1073–e1084 (2020).
76. T. Tsuboi, J. K. Wong, R. S. Eisinger, L. Okromelidze, M. R. Burns, A. Ramirez-Zamora, L. Almeida, A. Wagle Shukla, K. D. Foote, M. S. Okun, S. S. Grewal, E. H. Middlebrooks, Comparative connectivity correlates of dystonic and essential tremor deep brain stimulation. *Brain* **144**, 1774–1786 (2021).
77. E. H. Middlebrooks, L. Okromelidze, J. K. Wong, R. S. Eisinger, M. R. Burns, A. Jain, H.-P. Lin, J. Yu, E. Opri, A. Horn, L. L. Goede, K. D. Foote, M. S. Okun, A. Quiñones-Hinojosa, R. J. Uitti, S. S. Grewal, T. Tsuboi, Connectivity correlates to predict essential tremor deep brain stimulation outcome: Evidence for a common treatment pathway. *Neuroimage Clin* **32**, 102846 (2021).

Acknowledgments: We express our gratitude to S. Christie, PA-C, for her unwavering dedication to providing exceptional care for our patients. In addition, we extend our appreciation to the dedicated Radiology nurses and technologists at BWH whose expertise and commitment make these procedures possible. We also thank N. Li, N. Rajamani, L. Hart, S. Oxenford, and H. Friedrich for providing invaluable assistance and support throughout this project. **Funding:** This work was supported by National Institutes of Health grants R01MH113929 (M.D.F.), R21MH126271 (M.D.F.), R56AG069086 (M.D.F.), R21NS123813 (M.D.F.), R01NS127892 (M.D.F.), R01MH130666 (M.D.F.), UM1NS132358 (M.D.F.), R01 13478451 (A.H.), 1R01NS127892-01 (A.H.), 2R01 MH113929 (A.H.), and UM1NS132358 (A.H.); Neuronentics grant (M.D.F.); Kaye Family Research Endowment (M.D.F.); the Ellison/Baszucki Family Foundation (M.D.F.); Manley Family (M.D.F.); Focused Ultrasound Foundation grant (C.R.G.G.); the Schilling Foundation (A.H.). **Author contributions:** Conceptualization: M.D.F., G.R.C., C.N., J.D.R., M.M.J.C., and A.H. Methodology: M.D.F., G.R.C., J.D.R., K.B., M.M.J.C., T.A.D., A.H., and F.B. Resources: M.D.F., G.R.C., J.D.R., M.M.J.C., A.H., and A.M.P.. Funding acquisition: M.M.J.C., A.H., and A.M.P. Data curation: N.J.M., M.D.F., C.N., M.M.J.C., A.H., A.M.P., and A.B. Software: N.J.M., C.N., C.R.G.G., K.B., M.M.J.C., A.H., T.A.D., G.M.M., and A.M.P. Validation: M.D.F., G.R.C., C.N., J.D.R., M.M.J.C., and A.H. Formal analysis: M.D.F., K.B., M.M.J.C., and A.H. Project administration: M.D.F., G.R.C., M.M.J.C., and A.H.. Visualization: M.D.F., C.N., M.M.J.C., and A.H. Investigation: N.J.M., G.R.C., C.N., J.D.R., S.E.B., P.R.N., M.M.J.C., A.H., and F.B. Supervision: M.D.F., G.R.C., J.D.R., M.M.J.C., and A.H. Writing—original draft: C.N., M.M.J.C., and A.H. Writing—review and editing: N.J.M., M.D.F., G.R.C., C.N., J.D.R., S.E.B., C.R.G.G., P.R.N., M.M.J.C., T.A.D., A.H., F.B., A.M.P., A.B., A.Z.Y., M.S., J.G., N.L., and A.L. **Competing interests:** G.R.C. is a consultant for Insightec, which manufactures the MRgFUS equipment. M.D.F. has intellectual property on the use of brain connectivity imaging to analyze lesions and guide brain stimulation, and is a consultant for Magnus Medical, Soterix, Abbott, and Boston Scientific. A.H. reports lecture fees for Boston Scientific, was a consultant for FxNeuromodulation and Abbott in recent years and serves as a co-inventor on a patent granted to Charité University Medicine Berlin that covers multisymptom DBS fiberfiltering and an automated DBS parameter suggestion algorithm unrelated to this work (patent #LU103178). All other authors declare that they have no competing interests. **Data and materials availability:** All data needed to evaluate the conclusions in the paper are present in the paper and/or the Supplementary Materials.

Submitted 5 March 2024
Accepted 8 April 2025
Published 14 May 2025
10.1126/sciadv.adp0532